Differential Effects of Prenylation and *S*-Acylation on Type I and II ROPS Membrane Interaction and Function[1][W][OA]

Nadav Sorek[2], Orit Gutman, Einat Bar, Mohamad Abu-Abied, Xuehui Feng, Mark P. Running, Efraim Lewinsohn, Naomi Ori, Einat Sadot, Yoav I. Henis, and Shaul Yalovsky*

Department of Molecular Biology and Ecology of Plants (N.S., S.Y.) and Department of Neurobiology (O.G., Y.I.H.), George S. Wise Faculty of Life Sciences, Tel Aviv University, Tel Aviv 69978, Israel; Donald Danforth Plant Science Center, St. Louis, Missouri 63132 (X.F., M.P.R.); Department of Field and Vegetable Crops, Agricultural Research Organization, Neve Ya'ar Research Center, Ramat Yishay 30095, Israel (E.B., E.L.); Robert Smith Institute of Plant Sciences and Genetics of Agriculture, Faculty of Agriculture, Hebrew University of Jerusalem, Rehovot 76100, Israel (N.O.); and Department of Ornamental Horticulture, Agricultural Research Organization, Volcani Center, Bet-Dagan 50250, Israel (M.A.-A., E.S.)

Prenylation primarily by geranylgeranylation is required for membrane attachment and function of type I Rho of Plants (ROPs) and Gγ proteins, while type II ROPs are attached to the plasma membrane by *S*-acylation. Yet, it is not known how prenylation affects ROP membrane interaction dynamics and what are the functional redundancy and specificity of type I and type II ROPs. Here, we have used the expression of ROPs in mammalian cells together with geranylgeranylation and CaaX prenylation-deficient mutants to answer these questions. Our results show that the mechanism of type II ROP *S*-acylation and membrane attachment is unique to plants and likely responsible for the viability of plants in the absence of CaaX prenylation activity. The prenylation of ROPs determines their steady-state distribution between the plasma membrane and the cytosol but has little effect on membrane interaction dynamics. In addition, the prenyl group type has only minor effects on ROP function. Phenotypic analysis of the CaaX prenylation-deficient *pluripetala* mutant epidermal cells revealed that type I ROPs affect cell structure primarily on the adaxial side, while type II ROPs are functional and induce a novel cell division phenotype in this genetic background. Taken together, our studies show how prenyl and *S*-acyl lipid modifications affect ROP subcellular distribution, membrane interaction dynamics, and function.

Protein prenylation involves the covalent attachment of the C15 and C20 isoprenoids farnesyldiphosphate (FPP) and geranylgeranyldiphosphate (GGPP) to Cys residues in the C-terminal CaaX box or in C-terminal double Cys motifs of Rab small G proteins. Prenylation is required for membrane targeting and function of diverse protein groups, many of which have key regulatory functions (Maurer-Stroh et al., 2003, 2007; Magee and Seabra, 2005; Crowell and Huizinga, 2009; Sorek et al., 2009). Prenylation of CaaX box proteins is catalyzed by two distinct prenyltransferases: protein farnesyltransferase (PFT) and protein geranylgeranyltransferase-I (PGGT-I; Maurer-Stroh et al., 2003). PFT and PGGT-I are heterodimeric proteins composed of a common α-subunit and distinct substrate-specific β-subunits (Maurer-Stroh et al., 2003). Both PFT and PGGT-I are conserved in plants (Yalovsky et al., 1997; Caldelari et al., 2001). PFT and PGGT-I recognize a conserved C-terminal sequence known as the CaaX box, in which C is a Cys, a usually represents an aliphatic amino acid, and X is usually Ser, Met, Cys, Ala, Gln, or Leu. If X is a Leu, the protein is geranylgeranylated by PGGT-I. If X is another amino acid, the protein is preferentially farnesylated by PFT (Reiss et al., 1991; Seabra et al., 1991; Maurer-Stroh et al., 2003; Reid et al., 2004). The presence of an Arg/Lys-rich polybasic domain proximal to the CaaX box greatly increases substrate affinity of PGGT-I (James et al., 1995; Caldelari et al., 2001).

PFT and PGGT-I are in part promiscuous and PGGT-I can prenylate PFT substrates, albeit inefficiently (Trueblood et al., 1993; Armstrong et al., 1995;

[1] This work was supported by the Israel Science Foundation (grant no. ISF–312/07 to S.Y.), the United States-Israel Binational Research and Development Fund (grant no. BARD–IS–4032–07 to S.Y.), the Deutschland-Israel Program (grant no. DIP–H.3.1 to S.Y.), and by an Eshkol Fellowship for Ph.D. students from the Israel Ministry of Science and Technology to N.S. Y.I.H. is an incumbent of the Zalman Weinberg Chair in Cell Biology.

[2] Present address: Energy Biosciences Institute, University of California, Berkeley, CA 94720.

* Corresponding author; e-mail shauly@tauex.tau.ac.il.

The author responsible for distribution of materials integral to the findings presented in this article in accordance with the policy described in the Instructions for Authors (www.plantphysiol.org) is: Shaul Yalovsky (shauly@tauex.tau.ac.il).

[W] The online version of this article contains Web-only data.

[OA] Open Access articles can be viewed online without a subscription.

www.plantphysiol.org/cgi/doi/10.1104/pp.110.166850

Reid et al., 2004). PFT can prenylate most PGGT-I substrates but cannot use GGPP as a prenyl group donor (Reid et al., 2004). Mutations in the *PGGT-I* β-subunit gene (*Cdc43/Cal1*) are lethal in the budding yeast *Saccharomyces cerevisiae* (Trueblood et al., 1993). Knockout of the *PGGT-I* β-subunit gene in mouse leads to inhibition of K-Ras-induced cell proliferation and inhibition of lung tumor formation. Surprisingly, some mouse *pggt-Iβ* (*pggt-Ib*) knockout cell lines remained viable (Sjogren et al., 2007). Collectively, these data suggested that in vivo, PFT could partially compensate for the loss of PGGT-I activity but that PGGT-I also has unique critical functions.

Genetic studies in Arabidopsis (*Arabidopsis thaliana*) have shown that PFT and PGGT-I functions are essential for development and response to abiotic stress. The *enhanced response to aba* (*era1*) PFT β-subunit mutants are hypersensitive to abscisic acid during germination and show increased drought tolerance due to enhanced stomatal closure (Cutler et al., 1996; Pei et al., 1998; Allen et al., 2002). *era1* mutants also have increased shoot apical meristem (SAM), are late flowering, and are partially male sterile (Running et al., 1998; Bonetta et al., 2000; Yalovsky et al., 2000; Ziegelhoffer et al., 2000). *pluripetala* (*plp*), the shared PFT and PGGT-I α-subunit mutant, plants display severe growth and developmental alterations characterized by even more pronounced SAM expansion compared with *era1*, strongly retarded growth rate, and almost complete sterility (Running et al., 2004). Surprisingly, *pggt-Ib* mutants display only a subtle abscisic acid-hypersensitive phenotype and developmentally are not significantly different from wild-type plants (Johnson et al., 2005). In vitro assays of protein extracts from *pggt-Ib* mutant plants detected farnesylation but not geranylgeranylation. Furthermore, *era1 pggt-Ib* double mutants are phenotypically inseparable from *plp* (Johnson et al., 2005). Corresponding to the mild phenotype of *pggt-Ib*, only a minor mislocalization of the Gγ-subunit AGG1 was observed in the *pggt-Ib* background, while *plp* mutant plants showed accumulation of AGG1 in the soluble fraction (Zeng et al., 2007). Taken together, these data suggested that in Arabidopsis, PFT function could almost fully compensate for the loss of PGGT-I. However, it remained to be demonstrated that PGGT-I substrate proteins are indeed only farnesylated in the *pggt-Ib* background.

Rho of Plants (ROPs)/RACs are implicated in the regulation of diverse signaling cascades (Nibau et al., 2006; Yalovsky et al., 2008; Yang, 2008). For clarity, the ROP nomenclature will be used in this work. ROPs have been subdivided into two major subgroups designated type I and type II based on the amino acid sequences of their C-terminal hypervariable domains (Winge et al., 1997) and into three clades based on their nucleotide sequences (Fowler, 2010). Whereas type I ROPs terminate with a canonical prenylation CaaL box motif and are prenylated by PGGT-I, type II ROPs do not have a functional CaaX box prenylation motif and instead contain a plant-specific motif called the GC-CG box and are only *S*-acylated (Lavy et al., 2002; Lavy and Yalovsky, 2006; Sorek et al., 2007, 2009). An unrooted phylogram of 150 ROP coding sequences shows that type I *ROP* genes are divided into two clades, designated clades 1 and 3, whereas type II *ROP* genes constitute a single clade, designated clade 2 (Fowler, 2010). Clade 1 includes all four moss (*Physcomitrella patens*) and two lycophyte (*Selaginella moelendorfii*) ROP genes and is represented in Arabidopsis by *AtROP7* and *AtROP8*. Clade 3 includes most well-studied type I ROPs, namely *AtROP1*, *AtROP2*, *AtROP4*, and *AtROP6*, and also *AtROP3* and *AtROP5*. In Arabidopsis, clade 2 is presented by *AtROP9*, *AtROP10*, and *AtROP11* (Fowler, 2010). For clarity, given the focus of this study on the differential effects of C-terminal prenylation and *S*-acylation on ROP function, we will mostly refer to the division of ROPs into type I and type II based on their amino acid sequences.

Recently, we demonstrated that the Arabidopsis type I ROP, AtROP6 (ROP6), is transiently *S*-acylated on two G-domain Cys residues and that *S*-acylation affects membrane dynamics and function in the regulation of cell polarity (Sorek et al., 2010). The two *S*-acylated Cys residues are highly conserved; therefore, it is likely that other ROPs undergo similar activation-dependent *S*-acylation. The type I ROPs ROP2, ROP4, and ROP6 have been implicated in the regulation of pavement cell growth (Fu et al., 2002, 2005; Yang, 2008). ROP2 is also involved in root hair growth (Jones, 2002). ROP1, ROP3, and ROP5 are pollen specific, and the function of ROP1 in the regulation of pollen tube elongation has been studied in great detail (Yang and Fu, 2007; Yang, 2008). The normal-looking pavement cells, root hairs, and fertility of *pggt-Ib* mutant plants suggested that when ROPs are farnesylated (ROPs-F) instead of geranylgeranylated (ROPs-GG), their activity is not affected much, if at all. Since ROPs function primarily at the plasma membrane, the mild phenotype of *pggt-Ib* mutants suggested that subcellular distribution of ROPs-GG and ROPs-F could be similar. Alternatively, if similar to AGG1, a greater fraction of ROPs accumulates in the soluble fraction of the *pggt-Ib* mutant relative to wild-type plants, and the question arises whether the type of prenyl group affects the steady-state protein distribution between the plasma membrane and cytoplasm or the interaction dynamics with the plasma membrane. We have recently shown that the transient *S*-acylation of the G-domain affects the stability of ROP6 association with the plasma membrane and its partitioning into lipid rafts but not the steady-state distribution of the protein between the membrane and cytoplasm (Sorek et al., 2010). Hence, the contribution of prenylation and *S*-acylation to ROP function could be examined by studying ROP subcellular distribution, prenylation and *S*-acylation status, the resulting alterations in plasma membrane interaction dynamics, and the effects on cell polarity in both wild-type and *pggt-Ib* mutant plants.

Because type II ROPs are attached to the plasma membrane by *S*-acylation of hypervariable domain

GC-CG box Cys residues (Lavy et al., 2002; Lavy and Yalovsky, 2006), their function should not be compromised in the CaaX prenylation-deficient mutant *plp* and they might be responsible for the viability of this mutant. In yeast, ROP10 remained in the soluble fraction, while ROP9 was recruited to the plasma membrane and endomembrane by a farnesylation-dependent mechanism (Lavy et al., 2002), suggesting that the *S*-acylation mechanism of these proteins is plant specific. Thus, plants likely represent a special case where recruitment of some Rho GTPases to the plasma membrane takes place by a prenylation-independent mechanism. Previously, we showed that *plp* abaxial epidermis pavement cells have smaller lobes (Running et al., 2004), likely due to absent or only residual type I ROP function. The existence of lobes in the cells, however, indicates that cell polarity is maintained by other factors, possibly a redundant function of type II ROPs. The viability of the *plp* mutant plants provided us with an unprecedented opportunity to examine the redundancy and specificity of type I and type II ROP function in Arabidopsis.

In this study, we examined the specificity of type II ROP membrane attachment to plants by expressing type I and type II ROPs in mammalian cells and examining their localization and function. To explore the cross-specificity between PFT and PGGT-I, we directly analyzed the in vivo subcellular distribution and lipid modifications in wild-type *PGGT-IB* and *pggt-Ib* mutant plants of two protein substrates of PGGT-I: AGG1 (Zeng et al., 2007) and ROP6 (Sorek et al., 2007). To further define the function of prenylation and C-terminal *S*-acylation in ROP function, we examined the adaxial and abaxial pavement cell morphology in *plp* and the subcellular localization and function of the type II ROP AtROP11 in *plp*. We found how the type of prenyl lipid moiety affects the steady-state and membrane interaction dynamics of ROP6 and its function in the regulation of cell polarity as well as the specificity and redundancy between type I and type II ROPs.

RESULTS

Expression of Type I and Type II ROPs in Mammalian Cells

A representative from either subgroup of ROPs was expressed in NIH3T3 mammalian cells to examine the specificity of type II ROP C-terminal *S*-acylation to plants and the functional conservation of type I ROPs. Both the wild-type GFP-ROP6 and its constitutively active form GFP-rop6^{CA} were localized in the plasma membrane (Fig. 1, A and B). In the plasma membrane, GFP-rop6^{CA} was associated with lamellipodia enriched with phaloidine-labeled actin (Fig. 1, E–G, arrowheads in G). Interestingly, GFP-rop6^{CA} induced intercellular cell junctions in these fibroblast cells, where it was found to colocalize with β-catenin, a marker of cell-cell junctions (Fig. 1, H–J; note the yellow label in J, which corresponds to the colocalized proteins). Similar to activated mammalian Rac proteins, GFP-rop6^{CA} induced the formation of membrane ruffles (Fig. 1H, arrowheads; Supplemental Movie S1). In contrast to GFP-ROP6 and GFP-rop6^{CA}, the dominant negative mutant GFP-rop6^{DN} accumulated in aggregates inside the cells and was not detected at the plasma membrane (Fig. 1C). Different from either form of ROP6, the type II ROP, GFP-ROP9, was dispersed throughout the cytoplasm. Taken together, the data presented in Figure 1 indicated that ROP6 was recruited to the plasma membrane by prenylation and was able to interact with Rac effectors and induce signaling that led to the formation of lamellipodia, membrane ruffles, and cell-cell junctions. Membrane recruitment of ROP6 also depended on the ability of the protein to bind GTP and/or exchange nucleotides. The dispersal of GFP-ROP9 in the cytoplasm confirmed that recruitment of type II ROPs to the plasma membrane takes place by a plant-specific mechanism. Since the G-domains of type I and type II ROPs are highly similar (Berken and Wittinghofer, 2008), the functionality of ROP6 compared with ROP9 in the mammalian cells likely resulted from their ability to interact with the plasma membrane. Next, we examined the role of prenylation and prenyl group type on the function of ROPs.

ROPs and AGG1 Show Reduced Association with the Plasma Membrane in the *pggt-Ib* Mutant Background

It has been previously demonstrated that nonprenylated rop6^{C196S} and agg1^{C95S} mutants, in which the prenyl acceptor Cys residues were converted to Ser, accumulated in the soluble fraction (Sorek et al., 2007; Zeng et al., 2007). Furthermore, in *pggt-Ib*, AGG1 partially lost its association with the plasma membrane (Zeng et al., 2007). Confocal fluorescent images of leaf epidermis pavement cells show that, similarly, when expressed in *pggt-Ib* plants, a constitutively active His$_6$-GFP-rop6^{CA} (rop6^{CA}) was found in the plasma membrane, cytoplasm, and nuclei, while in wild-type *PGG-IB* plants, it was only detected in the membrane (Fig. 2A; Supplemental Movies S2 and S3). The plasma membrane localization of ROP6 in wild-type *PGG-IB* plants has been demonstrated previously (Sorek et al., 2007, 2010) and verified in this work by plasmolysis (Supplemental Fig. S1). Similar analyses were carried out with three independent transgenic lines for each genotype, and the results were the same. Supplemental Movies S2 and S3 show that in wild-type *PGG-IB* plants, no movement of rop6^{CA} through the cytoplasm could be detected (Supplemental Movie S2). In contrast, movement of rop6^{CA} through the cytoplasm was detected in *pggt-Ib* plants (Supplemental Movie S3).

Membrane flotation on Suc density gradients followed by immunoblot analysis was used to complement the fluorescence data (Fig. 2B). Quantification of

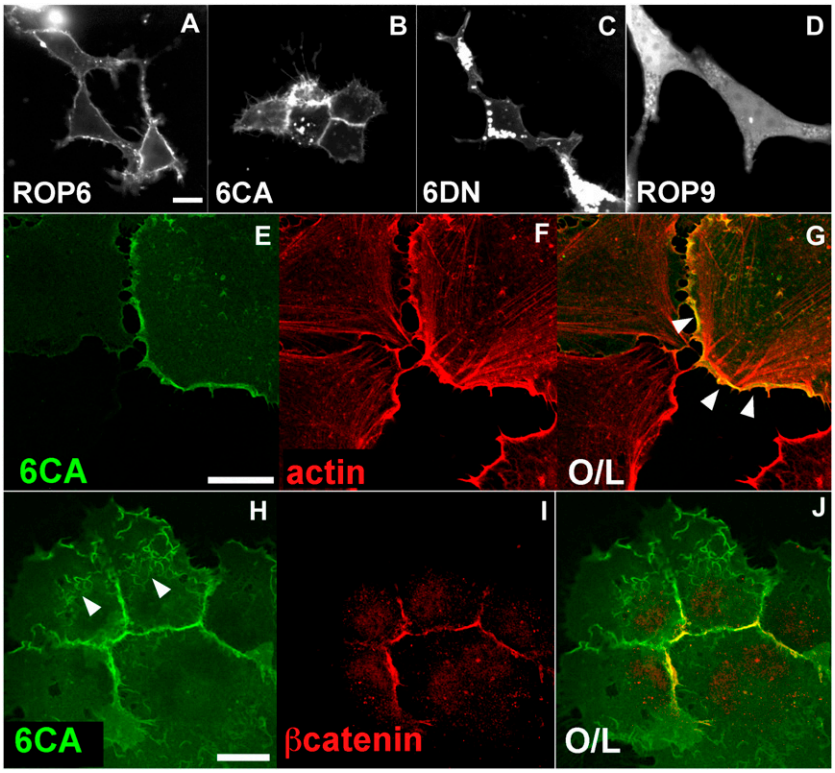

Figure 1. Expression of GFP-ROP6 and GFP ROP9 in NIH3T3 mammalian cells. The expressed proteins are as labeled: ROP6 (GFP-ROP6), 6CA (GFP-rop6^{CA}), 6DN (GFP-rop6^{DN}), and ROP9 (GFP-ROP9). Actin was labeled with phaloidine. O/L, Overlay. Arrowheads in G point to plasma membrane colabeled with GFP-rop6^{CA} and phaloidine-labeled actin. Arrowheads in H point to membrane ruffles. Bars = 10 μm.

the relevant bands is shown in Supplemental Figure S2. In the Suc gradients, the membrane fraction accumulated in fraction 3 from the top. In accord with previous reports (Sorek et al., 2007, 2010), protein immunoblots probed with anti-ROP6 antibodies showed that GFP-rop6^{CA} was exclusively localized in the plasma membrane in wild-type *PGGT-IB* plants. However, in *pggt-Ib*, it was detected in both membrane and soluble fractions (Fig. 2B; Supplemental Fig. S2). Immunoblots decorated with anti-GFP antibodies showed that a larger fraction of yellow fluorescent protein (YFP)-AGG1 was localized in the plasma membrane in wild-type *PGGT-IB* plants and that the amount of protein in the soluble fraction slightly increased in *pggt-Ib* (Fig. 2B; Supplemental Fig. S2), in line with previous findings (Zeng et al., 2007). Using the same anti-ROP6 antibodies, endogenous ROPs were only detected in the membrane fraction of wild-type *PGGT-IB* plants and in both membrane and soluble fractions in *pggt-Ib* protein extracts (Fig. 2B; Supplemental Fig. S2). The overall lower level of ROPs in the *pggt-Ib* background likely reflects the reduced stability of proteins. Thus, the loss of PGGT-I function similarly affected the subcellular distribution of recombinant GFP-rop6^{CA} and endogenous ROPs, leading to partial accumulation in the soluble fraction. Our previous findings showed that ROP6 is primarily geranylgeranylated and that in the *pggt-Ib* background a larger fraction of AGG1 is detected in the cytoplasm (Sorek et al., 2007; Zeng et al., 2007). These previous findings together with the data in Figure 2 suggested that PGGT-I is the primary enzyme responsible for membrane targeting of both type I ROPs and AGG1. The data further suggested that in *pggt-Ib*, ROPs and AGG1 are either not prenylated or farnesylated by PFT, leading to a partial loss of membrane targeting/interaction and to accumulation in the soluble fraction.

In Vitro Prenylation of ROP6

In vitro prenylation assays were carried out to assess the efficiency of ROP6 prenylation by PGGT-I and PFT (Fig. 3). Recombinant PGGT-I and PFT were expressed in baculovirus-infected insect cells (Caldelari et al., 2001), and ROP6 was expressed in *Escherichia coli* (Lavy et al., 2007). The purity of the recombinant proteins was verified with Coomassie Brilliant Blue-stained gels (Fig. 3A). ROP6 was prenylated more effectively by PGGT-I than by PFT, both qualitatively (Fig. 3B) and quantitatively, as determined by scintillation counting of [^{3}H]GGPP- or [^{3}H]FPP-labeled protein bands that were extracted from gels (Fig. 3, C and D). Comparison of the kinetic parameters shows that the K_m of PGGT-I toward ROP6 is approximately 10-fold lower than the K_m of PFT (0.16 versus 1.41 μM). The k_{cat} of ROP6 geranylgeranylation by PGGT-I is approximately 40-fold higher than the k_{cat} of its farnesylation by PFT (28.9 versus 0.71 min^{-1}). This is in line with the report that prenylation of AGG1 and AGG2 by PGGT-I is more efficient than by PFT (Zeng et al., 2007). These data suggest that, in vivo, ROPs and Gγ-subunits are prenylated by PGGT-I, but in its absence

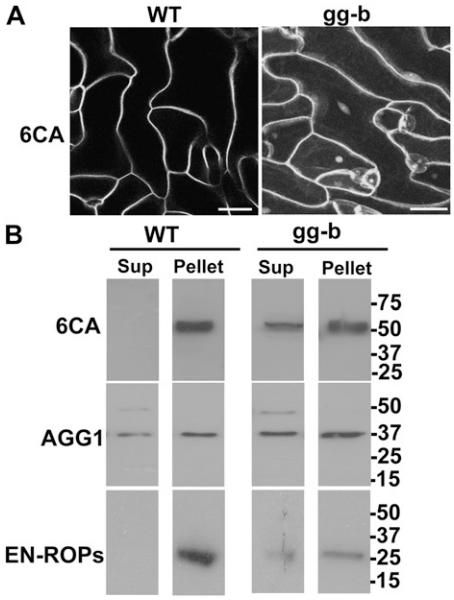

Figure 2. Subcellular localization of rop6^{CA} and AGG1. A, Fluorescence images showing the subcellular distribution of GFP-rop6^{CA} in wild-type Col-0 (WT) and *pggt-Ib* (gg-b) mutant leaf epidermis pavement cells. Note the nuclei and cytoplasmic strings in the *pggt-Ib* cells. Bars = 20 μm. B, Protein immunoblots decorated with anti-ROP polyclonal antibodies (6CA and EN-ROPs) or with anti-GFP monoclonal antibodies (AGG1). Soluble (Sup) and insoluble (Pellet) fractions were separated by floatation on Suc density gradients from wild-type Col-0 and *pggt-Ib* leaves. 6CA, GFP-His$_6$-rop6^{CA}; AGG1, YFP-AGG1; EN-ROPs, endogenous ROPs. Numbers on the side correspond to molecular mass in kD. Note the presence of rop6^{CA}, endogenous ROPs, and AGG1 in the soluble fractions in *pggt-Ib* extracts.

they are farnesylated by PFT. To examine this hypothesis, we purified recombinant rop6^{CA} and AGG1 from transgenic Arabidopsis plants and analyzed their modifying lipid moieties by gas chromatography-mass spectrometry (GC-MS).

Lipid Analysis of rop6^{CA} and AGG1 in Vivo

Recombinant rop6^{CA} and AGG1 were expressed in wild-type (ecotype Columbia [Col-0]) and *pggt-Ib* Arabidopsis plants. The proteins were purified from the membrane fraction (wild-type *PGGT-IB*) or from both the membrane and soluble fractions (*pggt-Ib*) using NH_4SO_4 precipitations, ion-exchange chromatography, and nickel-nitrilotriacetic acid (Ni-NTA) metal chelate chromatography. Lipids were released from the purified proteins as described previously (Farnsworth et al., 1990; Sorek et al., 2007) and in "Materials and Methods."

Hydrogenation, which is used in the lipid preparation procedure, reduces the prenyl double bounds, converting farnesyl and geranylgeranyl to 2,6,10-trimethyldodecane and 2,6,10,14-tetramethylhexadecane, respectively. For simplicity, we will refer to 2,6,10-trimethyldodecane as farnesyl (C15) and to 2,6,10,14-tetramethylhexadecane as geranylgeranyl (C20). Hydrogenation, which is carried out in the presence of ethanol and formic acid, also releases the acyl groups from proteins and promotes the formation of ethyl palmitate and ethyl stearate derivatives, which in turn can be efficiently analyzed by GC-MS (Sorek et al., 2007, 2010).

In wild-type *PGGT-IB* plants, rop6^{CA} was primarily geranylgeranylated (Fig. 4A; Supplemental Fig. S3), confirming earlier findings (Sorek et al., 2007). rop6^{CA}, which was purified from the *pggt-Ib* membrane fraction, was farnesylated but not geranylgeranylated,

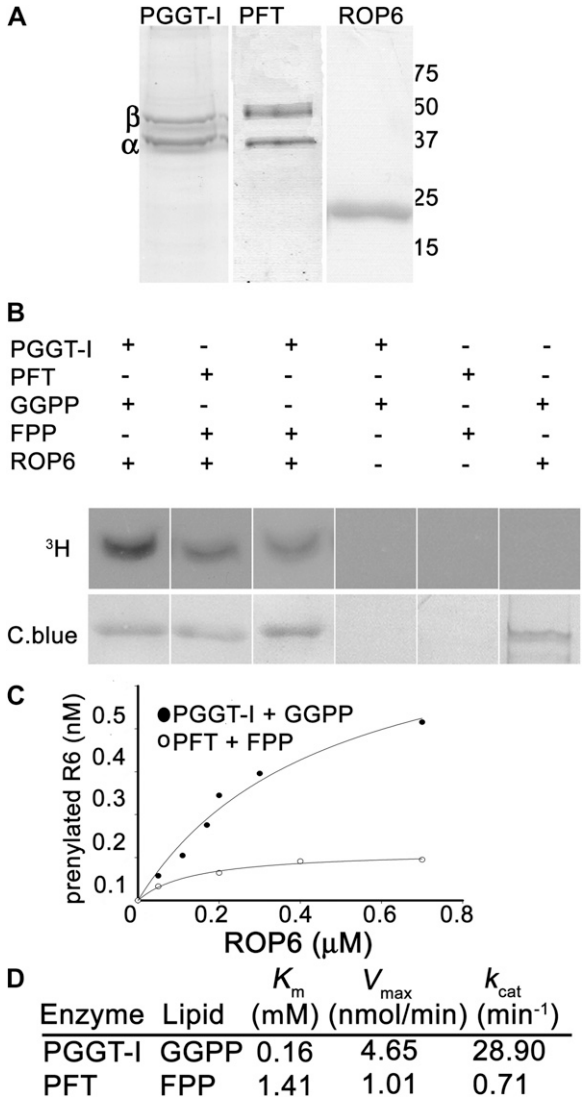

Figure 3. In vitro prenylation of ROP6 by PGGT-I and PFT. A, Stained SDS-PAGE gel showing purified recombinant PGGT-I, PFT, and ROP6. Numbers on the right correspond to molecular mass in kD. B, Fluorogram of in vitro prenylation reactions showing that ROP6 is preferentially prenylated by PGGT-I with GGPP as a prenyl group donor. C, Michaelis-Menten plots of prenylation of ROP6 by either PGGT-I or PFT with GGPP or FPP as prenyl group donor, respectively. D, Kinetic values calculated from the plots shown in C.

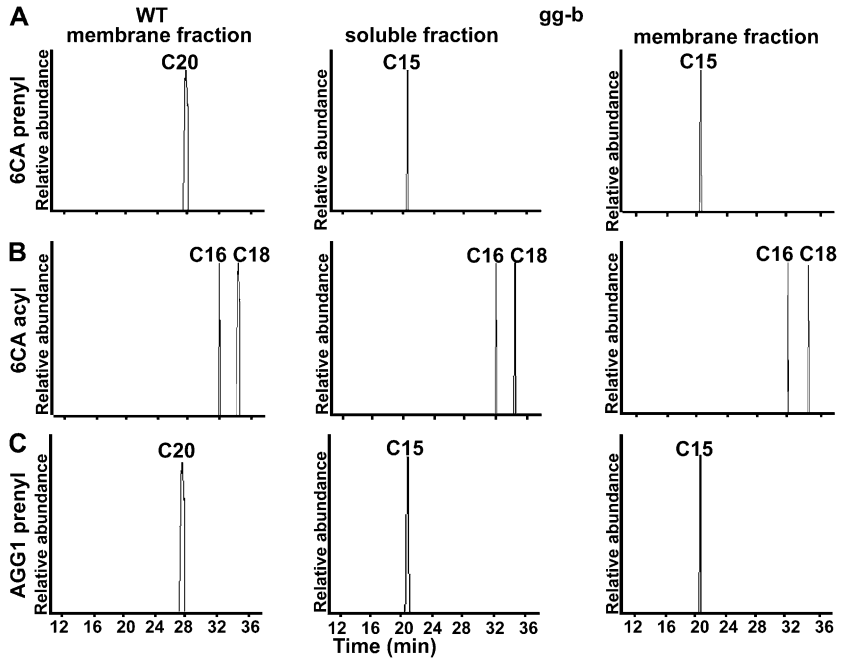

Figure 4. GC-MS analysis of soluble and insoluble rop6^{CA} and AGG1. A, In wild-type Col-0 (WT), rop6^{CA} was prenylated by geranylgeranyl (C20), while in *pggt-Ib* (gg-b), both soluble and membrane-associated rop6^{CA} were prenylated by a farnesyl group (C15). B, *S*-Acylation of rop6^{CA} by palmitic (C16) and stearic (C18) acids was the same in wild-type and *pggt-Ib* plants. Note that rop6^{CA} that was purified from the soluble fraction was also *S*-acylated. C, AGG1 is geranylgeranylated (C20) in wild-type plants and farnesylated (C15) in *pggt-Ib* plants. AGG1 is not *S*-acylated (Supplemental Figs. S3 and S4).

confirming the prediction that in the absence of PGGT-I, PFT prenylates ROP proteins. Interestingly, rop6^{CA} purified from the soluble fraction of *pggt-Ib* mutant plants was also farnesylated (Fig. 4A; Supplemental Fig. S3), indicating that the accumulation of ROPs in the soluble fraction was not due to their inefficient prenylation. This suggests either that targeting of the farnesylated rop6^{CA} to the membrane is less efficient or that its interaction with the membrane is less stable.

Similar to rop6^{CA}, AGG1 was only geranylgeranylated in wild-type plants and farnesylated in *pggt-Ib* mutants (Fig. 4C). Like rop6^{CA}, AGG1 isolated from the soluble fraction of *pggt-Ib* plants was farnesylated (Fig. 4C). The results with rop6^{CA} and AGG1, which are unrelated proteins, confirm that PGGT-I is the only CaaX geranylgeranyltransferase in Arabidopsis and that PFT can farnesylate diverse PGGT-I substrates. Taken together, due to the higher affinity of PGGT-I compared with PFT toward type I ROPs and AGG1, they are preferentially geranylgeranylated. However, the affinity of PFT toward type I ROP and AGG1 is sufficient for prenylating these proteins in the absence of PGGT-I function and thus for partially maintaining their attachment to the plasma membrane and function.

In wild-type *PGGT-IB* plants, rop6^{CA} was also *S*-acylated by palmitic (C16:0) and stearic (C18:0) acids (Fig. 4B; Supplemental Fig. S3), confirming our previous results (Sorek et al., 2007). *S*-Acylation was unaffected in the *pggt-Ib* mutant (Fig. 4B). Furthermore, in *pggt-Ib* plants, the membrane-associated rop6^{CA} partitioned into detergent-resistant membranes that could be lipid rafts (data not shown), similar to its partitioning in wild-type *PGGT-IB* plants (Sorek et al., 2007). Surprisingly, rop6^{CA} purified from the soluble fraction of *pggt-Ib* plants was also *S*-acylated (Fig. 4B). Because *S*-acylation likely takes place when ROP6 is localized in the plasma membrane, these results suggested that geranylgeranylation is required for stable steady-state plasma membrane localization. Neither the membrane-bound nor the soluble AGG1 proteins were *S*-acylated (Supplemental Fig. S4), in line with our previous results (Zeng et al., 2007).

Effect of the Prenyl Group on the Membrane Interaction Dynamics of ROP6

We have previously shown that the *S*-acylation of ROP6 is transient, occurs in the membrane, and depends on the activation status of the protein (Sorek et al., 2007, 2010). Thus, the farnesylated rop6^{CA} must first be targeted to the membrane to become *S*-acylated. Therefore, geranylgeranylation may affect either the steady-state distribution of ROPs between the plasma membrane and cytoplasm or the interaction dynamics of ROPs with the plasma membrane. To examine whether the type of the prenyl group affects the dynamics of the interactions of ROP proteins with the membrane, we used florescence recovery after photobleaching (FRAP) beam-size analysis (Henis et al., 2006). This technique enabled us to measure the dynamics of ROP6 and rop6^{CA} interactions with the plasma membrane of living cells.

The method employs FRAP with two different laser beam sizes, both small enough that diffusion in the cytoplasm is instantaneous and does not contribute to the measurement. FRAP beam-size analysis (Illenberger et al., 2003; Henis et al., 2006) explores the membrane interaction mode of proteins capable of both lateral diffusion in the membrane and exchange between membrane-associated and cytoplasmic pools. Typical

FRAP experiments are depicted in Figure 5A. Quantitative results on multiple cells using two different sizes of a Gaussian laser beam are shown in Figure 5, B and C. Two beam sizes were generated by focusing the Gaussian laser beam through a 63× objective (smaller Gaussian radius [ω]) or a 40× objective (larger ω), and the characteristic fluorescence recovery time (τ) values were determined with each. The ratio between the illuminated areas, $\omega^2(40\times)/\omega^2(63\times)$, was 2.28. When FRAP occurs by lateral diffusion, the ratio between the τ values measured with the two beam sizes, $\tau(40\times)/\tau(63\times)$, should equal the ratio between the illuminated areas; on the other hand, a τ ratio of 1 is indicative of recovery by exchange, which is a chemical relaxation process whose rate is independent of the beam size (Henis et al., 2006).

The fluorescence recovery mobile fraction values were high in all cases (0.93 or greater; Fig. 5A). Wild-type ROP6 exhibited a $\tau(40\times)/\tau(63\times)$ ratio of 2.0, close to but smaller than the 2.28 ratio typical of lateral diffusion (Fig. 5, B and C); this suggests that although the lateral diffusion of wild-type ROP6 is faster than its exchange and has a higher contribution to the FRAP, the exchange is not negligible and also contributes to the recovery (Niv et al., 2002; Illenberger et al., 2003; Rotblat et al., 2004; Henis et al., 2006). The constitutively active rop6^{CA} mutant recovered with a $\tau(40\times)/\tau(63\times)$ ratio of 2.3, suggesting recovery by pure lateral diffusion (Fig. 5, B and C). The τ ratio of rop6^{CA} in the *pggt-Ib* background was 1.9. Thus, although exchange contributed to the recovery, the lateral diffusion was faster and had a higher contribution to the FRAP (Fig. 5, B and C).

Thus, it appears that geranylgeranylation primarily affects the steady-state distribution of ROPs between the plasma membrane and cytoplasm and has only a minor effect on the association dynamics of ROPs with the membrane (Fig. 5). This, together with the subtle phenotype of the *pggt-Ib* mutant, suggests that the type of prenyl group has relatively small effects on ROP signaling. ROPs have been implicated in the regulation of cell polarity (Yang and Fu, 2007; Yalovsky et al., 2008), and their roles in the regulation of the structure of leaf epidermis pavement cells are well documented (Fu et al., 2002, 2005; Bloch et al., 2005). As the changes in epidermal cell morphology are simple to observe and quantify, we took advantage of this system to determine the effect of the prenyl group type on ROP signaling.

Effect of Prenyl Group Type on ROP-Regulated Cell Polarity

Images of typical leaf epidermis pavement cells are shown in Figure 6A. Differences in cell structure between nontransgenic wild-type (WT) and *rop6^{CA}* (6CA) cells and between His$_6$-GFP-ROP6 (6WT) and *rop6^{CA}* (6CA) cells are apparent. Cells of wild-type and ROP6 plants have many lobes, while the cells of the rop6^{CA}-expressing plants are more rectangular and have fewer and shallower lobes. Yet, the differences in the epidermal pavement cell structures between the wild type and *pggt-Ib* (gg-b), between the wild-type and ROP6, and between *rop6^{CA}* and *rop6^{CA} pggt-Ib* double mutants are more difficult to observe without quantification.

To quantify the differences in pavement cell structure, we used two ImageJ-based generated values called skeleton end points and circularity (Le et al., 2006) with modifications as described. The skeleton parameter turns the cell structure into lines and counts the number of end points. A single line with two end points would represent a cell without lobes. Thus, the minimal value of skeleton end points is always 2. The circularity parameter is defined by $(4\pi \text{ area})/(\text{perimeter}^2)$. Thus, for a circle, $(4\pi\ \pi r^2)/(2\pi r)^2 = 1$. For a given cell, circularity would have a value between 0 and 1. The circularity of a rectangular cell without lobes (similar to that of rop6^{CA}) would be closer to 1, whereas that of a cell with many deep and narrow lobes would be closer to 0. For clarity, the skeleton end points and circularity parameters were converted to "normalized skeleton" and "normalized circularity," respectively. Normalized skeleton = $(X - 2)/14$, where X is the number of skeleton end points. The maximal number of skeleton end points that we counted was 15 ($n \geq 500$ cells). We assume that in rare cases, this number could be higher. Thus, normalized skeleton = 1 in a cell with 16 skeleton end points and 0 in a cell without lobes. Normalized circularity = 1 – circularity. A plot of skeleton end point versus circularity shows an almost direct linear relationship between the two parameters (Supplemental Fig. S5C). Because normalized skeleton and normalized circularity also have the same scale and direction, they can be averaged. We designated average polarity score (APS) = normalized skeleton + normalized circularity/2 (Fig. 6B).

APS was calculated for 35 abaxial epidermal cells of seven different 14-d plants (examination of adaxial epidermal cells showed that their polarity was not different from that of abaxial cells). Wild-type cells had an average APS of 0.75 (Fig. 6B). *ROP6* (6WT) pavement cells had an average APS of 0.68 and were significantly different from wild-type nontransgenic plants ($P \leq 0.01$, ANOVA). The *pggt-Ib* (gg-b) pavement cells had an average APS of 0.69 and were significantly different from wild-type cells ($P \leq 0.01$, ANOVA) but not from *ROP6* cells. The *rop6^{CA}* (6CA) cells had an average APS of 0.17, indicating a large reduction in cell polarity. The *rop6^{CA} pggt-Ib* (6CA gg-b) double mutant cells had an average APS of 0.27, significantly different from 0.17 ($P \leq 0.01$, ANOVA). Thus, the analysis of cell structure shows that the lack of geranylgeranylation has significant but small effects on ROP-regulated cell polarity. Next, we examined cell polarity and type II ROP function in *plp* mutant plants that lack both PFT and PGGT-I function.

Function of Type II ROPs in *plp*

Images of adaxial and abaxial leaf epidermis in the wild type and *plp* are shown in Figure 7, A to D, and

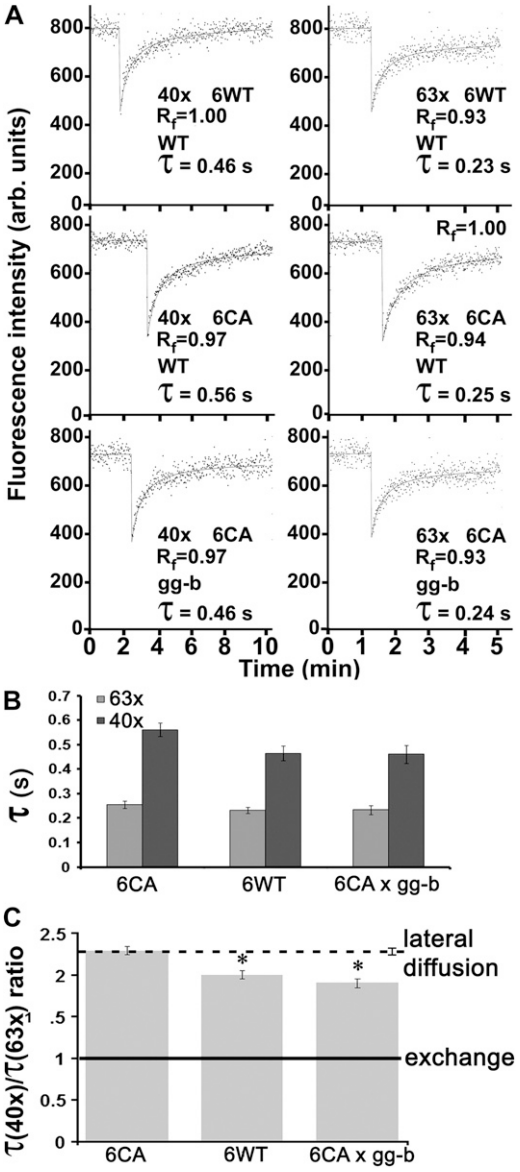

Figure 5. FRAP beam analysis of GFP-ROP6 and GFP-rop6^{CA} membrane dynamics in wild-type (WT) and *pggt-Ib* plants. A, Typical FRAP curves obtained with either 40× or 63× objectives for His$_6$-GFP-ROP6 (6WT), His$_6$-GFP-rop6^{CA} (6CA) in the wild type, or *pggt-Ib* (gg-b) leaf epidermis pavement cells. The solid lines show the best fit of a nonlinear regression analysis to the lateral diffusion equation (Petersen et al., 1986). The τ and mobile fraction (R_f) values derived for each specific curve are shown. B, Average τ values obtained with 40× (dark gray bars; ω = 1.17 μm) and 63× (light gray bars; ω = 0.77 μm) objectives. The $\omega^2(40\times)/\omega^2(63\times)$ ratio was 2.28. Bars are means of 35 measurements ± SE. No significant differences were obtained between the τ values of His$_6$-GFP-ROP6 (6WT) and His$_6$-GFP-rop6^{CA} (6CA) in cells from wild-type plants or between 6CA in wild-type versus *pggt-Ib* cells when comparing values measured with the same objective (Student's *t* test). C, Ratios of the τ values shown in A. The dashed line and the solid line correspond to FRAP by pure lateral diffusion or pure exchange, respectively. The τ ratios, beam-size ratio, and their SE were calculated from the experimentally measured τ and ω^2 values using bootstrap analysis. This analysis showed that the τ ratios of wild-type ROP6 in cells from wild-type plants (6WT) and of rop6^{CA} in cells from *pggt-Ib* plants (6CA × gg-b) differed significantly from the 2.28 beam-size ratio predicted for FRAP by lateral diffusion (* $P \leq 0.02$, bootstrap analysis).

quantification of skeleton end points, circularity, and APS are shown in Figure 8, A to C. The adaxial *plp* pavement cells had very few lobes (Fig. 7B), having on average 3.6 skeleton end points (Fig. 8B). The average circularity value of the *plp* adaxial cells was 0.53, and their APS value was 0.29 (Fig. 8C). In comparison, wild-type adaxial cells had on average 12.2 skeleton end points, an average circularity value of 0.22, and an average APS of 0.75 (Figs. 7A and 8C). The differences between the wild type and *plp* in the number of skeleton end points, circularity, and APS values were significant ($P \leq 0.01$, Tukey-Kramer ANOVA). The effect of the *plp* mutation on the abaxial pavement cells was milder, with cells developing many lobes (Fig. 7, C and D). On average, *plp* abaxial pavement cells had 9.3 skeleton end points, circularity of 0.28, and APS of 0.63 versus 12.2, 0.22, and 0.75 in wild-type cells, respectively (Fig. 8C). The reduced polarity of *plp* pavement cells is well in agreement with the role of type I ROPs in the regulation of cell growth. At the same time, the differences between adaxial and abaxial pavement cells indicate that their growth is regulated by partially distinct mechanisms. *plp* abaxial pavement cells are on average significantly larger ($P \leq 0.0005$, Student's *t* test), with an average area of around 6,000 μm^2 compared with around 2,500 μm^2 in wild-type cells (Fig. 8D). In addition, the *plp* abaxial pavement cells have a wider range of sizes (compare Fig. 7, C and D, and the error bars in Fig. 8D). Another notable difference is the reduced density of stomata in *plp* abaxial epidermis. In wild-type abaxial epidermis, there are on average 60 stomata per 185 mm^2, whereas in *plp*, there are around 20 stomata per 185 mm^2 ($P \leq 0.005$, Student's *t* test). Similar variability in the cell sizes and stomata density was also observed in the *plp* adaxial epidermis (Fig. 7, A and B). Hence, in addition to cell growth, *plp* is also affected in cell division. Since type II ROPs are likely functional in *plp*, they may be responsible for the viability of the mutant plants. In addition, it could be that the phenotype of *plp* plants also results from an imbalance between the activities of type I and type II ROPs. The following series of experiments addressed these hypotheses.

A constitutively active GFP-rop11^{CA} (rop11^{CA}) mutant (Bloch et al., 2005) was expressed in *plp* to examine the function of type II ROPs in a CaaX prenylation-deficient background (Fig. 7, E–H). In *plp* as in wild-type plants (Bloch et al., 2005), rop11^{CA} was localized in the plasma membrane (Fig. 7, F–H), confirming that targeting and association of type II ROPs with the membrane are unaffected in the absence of prenylation. Abaxial cells expressing the rop11^{CA} mutant were rectangular or cubical (Fig. 7E) and were different in their morphology compared with abaxial *plp* pave-

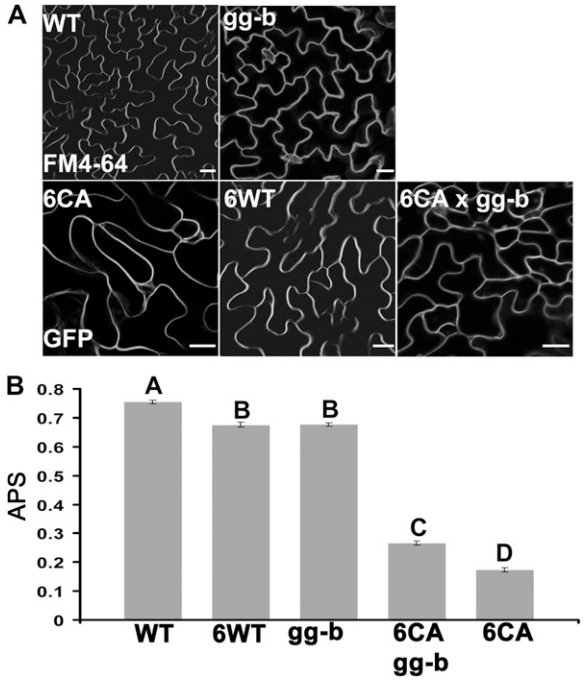

Figure 6. The requirement for geranylgeranylation in ROP-regulated cell polarity. The effect on cellular polarity was measured on leaf epidermal cells. A, Typical epidermal cells of the wild type (WT), *pggt-Ib*, *rop6*^{CA}, and *rop6*^{CA} *pggt-Ib*. In nontransgenic wild-type and *pggt-Ib* (gg-b) plants, cells were labeled with FM4-64. In ROP6 (6WT) and *rop6*^{CA} (6CA) transgenic plants, cells were visualized with by GFP. Bars = 20 μm. B, APS of epidermal pavement cells. Letters above bars indicate significant differences ($P \leq 0.01$, ANOVA). Error bars indicate SE. Note the lower APS values of *pggt-Ib* (gg-b) and ROP6 (R6) cells compared with wild-type cells and the higher APS values of *rop6*^{CA} *pggt-Ib* (6CA gg-b) compared with *rop6*^{CA} (6CA).

ment cells (Fig. 7D). In addition, rop11^{CA} induced ectopic symmetric and asymmetric cell divisions resulting in many developing stomata. We have not observed this phenotype when either ROP11 or other activated ROP mutants were expressed in the wild-type background (Lavy et al., 2002; Bloch et al., 2005; Sorek et al., 2007, 2010). Hence, the ectopic cell divisions resulted from expression of the activated ROP in the *plp* background. The functionality of type II ROPs in *plp* suggests that they may indeed substitute in part for the loss of type I ROP function, facilitating the viability of this mutant. These results also revealed a function for ROPs in the regulation of cell division and suggest that the GFP-rop11^{CA} gain-of-function phenotype is balanced by the function of other prenylated proteins, possibly type I ROPs.

DISCUSSION

The function of ROP GTPases depends on C-terminal stable prenylation or *S*-acylation and on activation-dependent transient *S*-acylation in the G-domain. The association of GFP-rop6^{CA} with actin enriched lamellipodia, and its capability to induce membrane ruffles and cell-cell junctions (Fig. 1) resembles the activities of mammalian Rac (Jaffe and Hall, 2005) and its GEF Tiam1 (Hordijk et al., 1997; Uhlenbrock et al., 2004). Hence, it is likely that ROP6 can interact with Rac effectors. Despite the differences in the insert domains of ROPs and mammalian Racs (Berken and Wittinghofer, 2008), Rac/ROP-interacting proteins contain domains such as the Cdc42 Rac-interacting binding domain (Wu et al., 2001), which is conserved in eukaryotes. Therefore, although most of the mammalian Rac effector proteins do not exist in plants, ROPs could presumably interact with some of them. Because type I ROPs are prenylated, they can be recruited to the plasma membrane, depending on their ability to bind GTP, and become active. The recruitment of wild-type ROP6 to the plasma membrane of

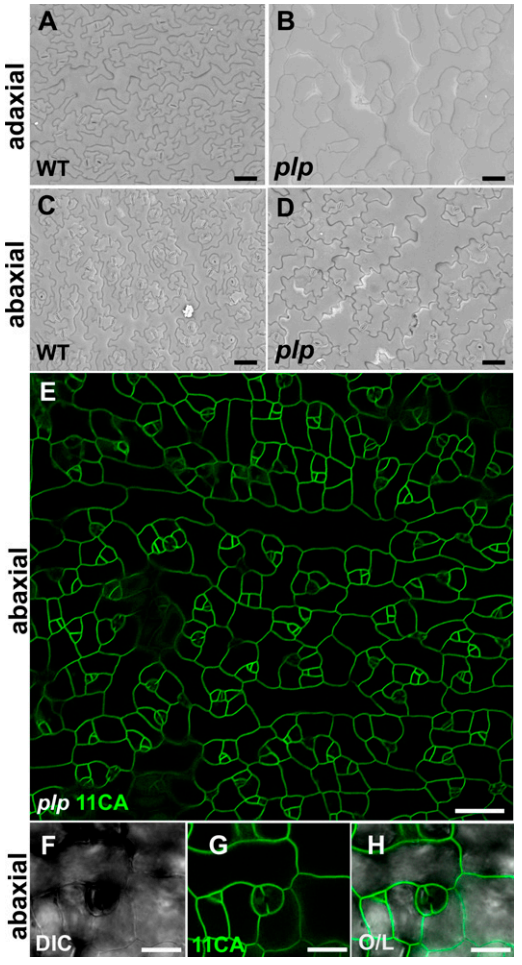

Figure 7. *plp* leaf epidermis and expression of GFP-rop11^{CA} in *plp*. A to D, Adaxial and abaxial leaf epidermis of wild-type (WT) Col-0 and *plp*. E to H, Expression of GFP-rop11^{CA} (11CA) in *plp* abaxial epidermis. E and F are fluorescent images, F is a Nomarsky differential interference contrast (DIC) image, and H is a fluorescent/DIC overlay (O/L) image. Bars = 20 μm.

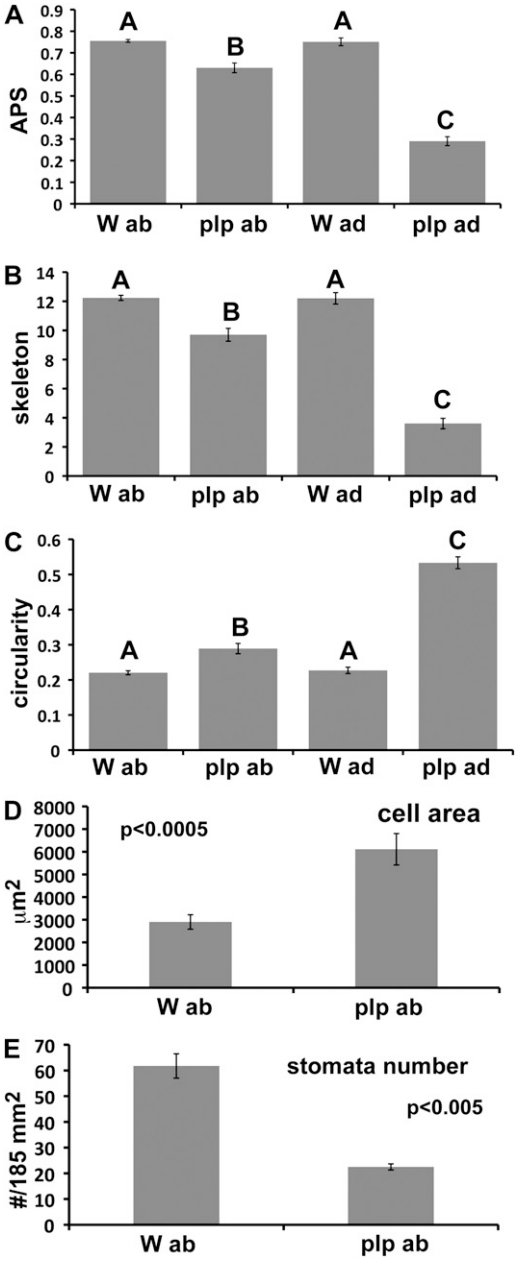

Figure 8. Polarity, cell area, and stomata density in wild-type Col-0 (W) and *plp* leaf epidermis. Error bars correspond to SE. In A to C, letters above the bars correspond to significant differences as determined by Tukey-Kramer ANOVA ($P \leq 0.01$). Statistical analysis in D and E was carried out with Student's *t* test.

NIH3T3 cells indicates that it could interact with and be activated by the mammalian RhoGEFs, as would be expected from in vitro studies (Berken et al., 2005; Basu et al., 2008). Type II ROPs are almost identical to type I ROPs in the catalytic G domain, but the mechanism of their recruitment to the plasma membrane is plant specific, and hence they remain inactive. In the future, elucidation of the Rac effectors that interact and are activated by type I ROPs could be used as a basis for an evolution-based structure-function analysis of the Rho GTPase signaling module.

The analysis of prenylation and *S*-acylation in vivo demonstrated how each of these modifications affects the steady-state distribution of ROPs in the cell, their membrane interaction dynamics, and function. Recently, we have demonstrated that transient *S*-acylation of G-domain Cys residues is required for ROP membrane dynamics and signaling in cell polarity (Sorek et al., 2010). In this work, we show that the type of prenyl group affects the steady-state distribution of ROPs between the plasma membrane and the cytoplasm, but only to a limited extent are ROP membrane dynamics and signaling affected in cell polarity. Owing to their recruitment to the plasma membrane by *S*-acylation, type II ROPs remain functional in the *plp* CaaX protein prenylation-deficient mutant and may partially suppress the loss of type I ROP function in the regulation of cell polarity, revealing both unique and partial functional redundancy of the two ROP subgroups. The analysis of protein prenylation by GC-MS (Fig. 4) shows that although the k_{cat} of PGGT-I toward ROP6 is 40 times higher than the k_{cat} of PFT (Fig. 3), in vivo, PFT can substitute PGGT-I. The GC-MS analysis also shows that ROP6 and AGG1 purified from the soluble fraction of *pggt-Ib* were farnesylated (Fig. 4, A and C). This indicates that the accumulation of the CaaL box containing PGGT-I protein substrates in the soluble fraction in *pggt-Ib* mutant plants is not the result of inefficient prenylation by PFT. The surprising identification of farnesylated and *S*-acylated forms of rop6^{CA} in the soluble fractions indicates that the combination of farnesyl in the hypervariable domain and acyl group(s) in the G-domain does not ensure stable steady-state association with the plasma membrane. The functionality of farnesylated ROP forms may explain the relatively subtle phenotype of the *pggt-Ib* mutant plants (Johnson et al., 2005; Zeng et al., 2007). Yet, under some growth conditions, the requirement for efficient prenylation and stable interaction with the plasma membrane could become critical, explaining why PFT and PGGT-I have been conserved in plants.

The reduced steady-state association of ROPs with the plasma membrane in *pggt-Ib* (Fig. 2; Supplemental Movie S3) resulted in a minor decrease in the $\tau(40\times)/\tau(63\times)$ ratio of rop6^{CA} from 2.3 in wild-type cells to 1.9 in *pggt-Ib* (Fig. 5). The lateral diffusion always has a higher contribution to the measured FRAP at the smaller beam size (63×), where diffusion occurs faster relative to exchange (Henis et al., 2006). Hence, comparison of the $\tau(63\times)$ values could highlight differences in the lateral diffusion of the protein in the membrane under different conditions or genetic backgrounds. The $\tau(63\times)$ values measured for rop6^{CA} in the wild type and in *pggt-Ib* were essentially similar (Fig. 5B). This indicates that the lateral mobility rop6^{CA} in the plasma membrane of cells from wild-type and *pggt-Ib* cells is similar. Taken together, the FRAP beam-size analysis indicates that the type of prenyl group

has only minor effects on the membrane interaction dynamics of ROPs.

ROPs undergo transient *S*-acylation by palmitic and/or stearic acids and consequential partitioning into detergent-resistant membranes that could be lipid rafts (Sorek et al., 2007, 2010). It was shown that *S*-acylation takes place on two highly conserved G-domain Cys residues, Cys-21 and Cys-156. The $\tau(40\times)/\tau(63\times)$ ratio of a rop6^{CA} C21S/C156S double mutant (rop6$^{CA21+156mSS}$) exhibited a highly significant shift to 1.4 (Sorek et al., 2010), suggesting that this mutation slowed down its lateral diffusion and elevated the exchange rate, resulting in a higher contribution of exchange to the FRAP. Furthermore, overexpression of the rop6$^{CA,C21S/C156S}$ had only small effects on cell polarity (Sorek et al., 2010), indicating that *S*-acylation, partitioning into lipid rafts, and stable association with the plasma membrane are required for the regulation of cell polarity by ROPs. Prenylation is required for initial targeting of type I ROPs to the membrane (Sorek et al., 2007), presumably for their interaction with RhoGDI (Boulter and Garcia-Mata, 2010) and for the steady-state distribution of ROPs between the plasma membrane and cytoplasm. Once in the membrane, ROP function is modulated by activation-dependent transient *S*-acylation that likely affects protein conformation (Sorek et al., 2010). rop6^{CA} was *S*-acylated in *pggt-Ib*; therefore, its membrane interaction dynamics was between wild-type and mutant backgrounds. The minor effects on ROP function in *pggt-Ib* could be explained by the overall reduction in the levels of ROPs at the plasma membrane. The lower levels of ROPs in *pggt-Ib* may be due to the degradation of misplaced ROPs that accumulated in the cytoplasm, as have been shown for Rho proteins in yeast and mammalian cells (Boulter et al., 2010). It was shown that RhoGDI protects prenylated Rho proteins from degradation (Boulter et al., 2010). Both gernaylgeranylated and farnesylated Rho were shown to interact with RhoGDI (Michaelson et al., 2001); however, based on structural considerations, ROPs-F are expected to have lower affinity to RhoGDI compared with ROPs-GG (Hoffman et al., 2000; Scheffzek et al., 2000; Grizot et al., 2001). In addition, *S*-acylation may function as a RhoGDI displacement factor (Michaelson et al., 2001). Taking into account these considerations, it is likely that in the *pggt-Ib* plants most ROPs-F are not associated with RhoGDI, leading to their degradation.

Prenyl groups are as hydrophobic as acyl chains but are relatively rigid, since they contain double bonds and a bulky methyl side chain for every four-carbon atom along the main chain. These features also render prenyl groups less packed than acyl chains. These differences suggest that prenyl and acyl moieties may interact with the membrane in different fashions. One possibility is that the prenyl groups are not directly embedded in the lipid bilayer but instead interact with membrane-associated factors that could function as receptors (Belanis et al., 2008). Such specific receptors for geranylgeranylated proteins could account for the reduced stability in the membrane of farnesylated and *S*-acylated ROPs (Figs. 2–4). An indirect interaction of prenylated proteins with the membrane could also explain the relatively minor effect of the prenyl group type on ROP membrane dynamics (Fig. 5).

Mammalian RhoB is both farnesylated (RhoB-F) and geranylgeranylated (RhoB-GG), and the specific function of each form is unclear (Prendergast, 2001). In the budding yeast *S. cerevisiae*, overexpression of Cdc42, a PGGT-I substrate, can overcome the lethality of *pggt-Ib* (*cdc43*Δ) mutants (Trueblood et al., 1993), suggesting that a farnesylated Cdc42 is functional to a certain extent. In the fission yeast *Schizosaccharomyces pombe*, PGGT-I is dispensable for cell viability under permissive temperatures (Díaz et al., 1993), and some mammalian *pggt-Ib* knockout cell lines remained viable (Sjogren et al., 2007). As mentioned above, Arabidopsis *pggt-Ib* mutants have only subtle phenotypes (Johnson et al., 2005). Thus, it appears that the specific requirement for PGGT-I is cell specific and species specific. Importantly, as revealed in this work, the membrane interaction dynamics and lateral mobility of rop6^{CA}-F and rop6^{CA}-GG, and possibly other geranylgeranylated proteins, display only minor differences. Thus, in the absence of PGGT-I activity, when the physiological conditions allow, farnesylation of PGGT-I substrates by PFT is sufficient for their function, maintaining cell and organism viability.

In *plp*, in the absence of prenylation, plant viability may be facilitated by a unique mechanism of stable C-terminal *S*-acylation of type II ROPs (Figs. 1, 7, and 8). In addition, at present, we cannot exclude that residual type I ROP function is maintained due to arbitrary interaction of these proteins with the plasma membrane. This residual activity of type I ROPs, in addition to type II ROPs, may explain the severe but incomplete male sterility and the few lobes and indentations that are formed on the adaxial pavement cells. The degree of identity between type I and type II ROPs in the catalytic G-domain is above 90%. Hence, it is likely that they can interact with a similar set of effector molecules. Yet, the changes in cell structure in *plp* indicate that type I and type II ROPs may be targeted to different domains in the plasma membrane or that they are differentially expressed. Microarray data from Genevestigator (Hruz et al., 2008) indicate that the type I ROPs ROP2, ROP4, and ROP6 and all three type II ROPs are expressed at low levels in early and mature leaves (Supplemental Fig. S6). Expression, however, could be confined to different cell types.

Prenylation is required for Rho interaction with RhoGDI under physiological conditions (Hoffman et al., 2000; Scheffzek et al., 2000; Grizot et al., 2001), and palmitoylation (*S*-acylation) was suggested to function as a RhoGDI displacement factor (Michaelson et al., 2001). Possibly, therefore, type II ROPs do not interact with RhoGDI. Since type I ROPs cannot be prenylated in *plp*, they are unlikely to interact with RhoGDI, a fact that may facilitate their instability. It

has been demonstrated that RhoGDIs are involved in the regulation of ROP function and cell polarity in tip growth. In tobacco (*Nicotiana tabacum*) pollen tubes, RhoGDI was shown to facilitate recycling of ROPs to the growing tip (Klahre et al., 2006). In Arabidopsis, a loss-of-function mutant in the RhoGDI *SCN1* gene developed root hairs with multiple tips in which ROP2 was mislocalized. Hence, in addition to differential expression, the ability of ROPs to interact with RhoGDI may affect cell polarity in *plp*. Future studies will have to address whether type II ROPs interact with RhoGDI and how they regulate cell polarity.

The differences in cell structure on the adaxial and abaxial sides of *plp* leaves suggest that cell growth on both side of the leaf is regulated by partially nonoverlapping mechanisms. The stronger change in cell polarity on the adaxial side may reflect a greater contribution of type I ROP to cell growth on this side of the leaf. Alternatively, ROPs may interact with different pathways to control cell growth on the adaxial and abaxial leaf sides. Interestingly, mutants of the ROP effector ICR1 have altered epidermal cell morphology on the adaxial epidermis (Lavy et al., 2007). Adaxial/abaxial leaf polarity is set up early during leaf development by a signal coming from the SAM, and mutations in transcriptional regulators of adaxial/abaxial cell identity or disruption of their expression lead to the development of radialized leaves instead of flat laminas (Efroni et al., 2010). It has recently been reported that loss of all *YABBY* gene activities led to the development of dorsiventral structures, which resulted from failure to activate the *CINCINNATA*-class *TCP* genes and compromised auxin and the PIN1 auxin efflux carrier distribution (Sarojam et al., 2010). The development of flat leaf laminas should require coordinated growth of the leaf cells, a process that involves regulation by ROPs (Fu et al., 2005). We have recently demonstrated that ICR1 is required for the recruitment of PIN proteins to polar domains in the plasma membrane (Hazak et al., 2010), linking PIN-regulated auxin transport with ROP-modulated cell polarity.

The expression of rop11^{CA} in *plp* revealed a role for ROPs in the induction of cell division (Fig. 7E). The ectopic cell divisions in the *plp rop11*^{CA} leaves also suggest that other prenylated proteins balance ROP function. It could be that the reduction in stomata numbers, the increase in average cell size, and the slow growth rate of *plp* reflect reduced functions of type I ROPs. The phenotype of *plp* and the effect of rop11^{CA} on cell division in the *plp* background suggest that intricate type I and type II ROP activation/inactivation equilibrium is coordinated with or modulated by the genetic network that regulates adaxial/abaxial cell fate.

MATERIALS AND METHODS

Plant Material

Wild-type Col-0 and *pggt-Ib*, *plp*, and *plp GFP-rop11*^{CA} mutants and transgenic Arabidopsis (*Arabidopsis thaliana*) plants were grown in 5-cm pots on soil (Marom Golan mix) and irrigated from below. Plants were grown under long-day conditions (16-h-light/8-h-dark cycle) at 21°C. The light intensity was 100 μE m^{-2} s^{-1}. Analyses of transgenic plants were carried out with three independent transgenic lines for each genotype.

Molecular Cloning

The *ROP* cDNAs were ligated to the Clontech mammalian expression vector pLPCX that was modified as follows. A cDNA of the improved, higher fluorescence Venus version of YFP (Nagai et al., 2002) was inserted between *Xho*I and *Hin*dIII of the pLPCX multiple cloning site. A linker of Gly-Ser-Thr-Ser-Gly was added downstream to the YFP. The *ROP* cDNAs were ligated in-frame to YFP between *Eco*RI and *Cla*I.

Protein Expression in *Escherichia coli* and Baculovirus-Infected Insect Cells

E. coli DH5α was used for DNA propagation. For protein expression in *E. coli*, His$_6$-ROP6 (*pSY804*; Sorek et al., 2007) was transformed into *E. coli* BL21 CodonPlus DE3 RIL cells (Stratagene). Cells were grown to an optical density at 600 nm of 0.6, and then protein expression was induced by adding 2 mM isopropyl-β-D-thiogalactopyranoside and growth at 25°C for 2 h. Protein extraction and purification on Ni-NTA columns was performed according to the manufacturer's instructions (Qiagen).

PGGT-I and PFT were expressed in baculovirus-infected insect cells and purified as described previously (Caldelari et al., 2001). Typically, 4×10^6 *SF9* cells were infected with 10^9 viral particles 24 h after splitting. To express PFT, cells were coinfected with viruses harboring PFTB and PFTA/PGGT-I cDNAs. To express PGGT-I, cells were coinfected with viruses harboring the PGGT-I and PFTA/PGGT-I cDNAs. After 72 h, cells were harvested and the heterodimeric His$_6$-tagged PFT or PGGT-I proteins were purified over an Ni-NTA column according to the manufacturer's instructions (Qiagen).

Prenylation Reactions

Prenylation reactions were performed essentially as described (Caldelari et al., 2001). Typical reactions contained 0.5 pmol (0.01 μM) of purified PGGT-I or PFT, 0.8 μM all-trans [^{3}H]GGPP or [^{3}H]FPP (30 Ci mmol^{-1}; American Radiolabeled Chemicals), 0.2 μM ROP6, 50 mM HEPES-KOH, pH 7.8, 5 mM $MgCl_2$, 50 μM $ZnCl_2$, 2.5 mM dithiothreitol, and 0.3% [v/v] Nonidet P-40 in a total volume of 25 μL. Protein concentrations were determined using the bicinchoninic acid kit (Pierce) and by absorption at 280 nm. All ingredients except the enzyme were mixed and kept on ice. The enzyme was then added, and each mix was incubated at 30°C for 30 min. Reactions were carried out in triplicate and were terminated by adding SDS-PAGE denaturing buffer. Equal amounts of proteins were resolved by SDS-PAGE. A lane with a nonmodified ROP6 protein was run next to each reaction. The gels were briefly stained with Coomassie Brilliant Blue; gel slices harboring the radiolabeled proteins were identified according to the stained protein bands, excised from the gels, cut into pieces, and incubated in scintillation liquid for 48 h, followed by measuring the radioactivity in a scintillation counter.

Protein Immunoblots

Anti-ROP6 antibodies (Sigma R9529, lot 106K4831) were used at a dilution of 1:3,000 together with blotting-grade horseradish peroxidase-conjugated goat anti-rabbit IgG (Bio-Rad). Anti-GFP monoclonal antibodies (Covance) were used at a dilution of 1:3,000 followed by horseradish peroxidase-conjugated goat anti-mouse IgG (Bio-Rad). Detection was with EZ-ECL (Biological Industries). Quantification of protein bands was done with ImageJ (http://rsbweb.nih.gov/ij/).

Protein Extraction and Purification from Plants

To prepare protein extracts containing His$_6$-GFP-rop6^{CA} or YFP-AGG1, 15 g of rosette leaves from 2-week-old transgenic plants was harvested and batch frozen in liquid N_2. Proteins were extracted from the frozen leaves by grinding with a pestle and mortar in 3× volumes (45 mL) of plant extraction buffer (50 mM NaH_2PO_4, pH 7.6, 2 mM $MgCl_2$ [only in extraction ROP6], 300 mM NaCl, 10% glycerol, 2 mM β-mercaptoethanol, and plant protease inhibitor mixture [Sigma]). To precipitate insoluble material, homogenates were centrifuged at

75,000*g* for 30 min. The resulting supernatants (soluble fraction) were collected for further analysis, and the insoluble pellet was incubated on ice for 30 min in the same volume (45 mL) of plant extraction buffer containing 1% Triton X-100 and 0.1% SDS. Extracts were centrifuged at 75,000*g* for 30 min. The resulting supernatant representing the membrane fraction was collected for further analysis.

His_6-GFP-ROP6 proteins were purified from total protein extracts by a two-step procedure: (1) a differential NH_4SO_4 precipitation (Ausubel et al., 1995); and (2) purification over a Ni-NTA column. In the NH_4SO_4 precipitation, His_6-GFP-rop6^{CA} proteins were precipitated in the 30% to 45% NH_4SO_4 fraction. The precipitates were dissolved and dialyzed against 50 mM NaH_2PO_4, pH 6.0, 300 mM NaCl, 2 mM β-mercaptoethanol, and 0.2% Tween 20. The dialyzed fractions were collected, and the His_6-GFP-rop6^{CA} proteins were purified over a 0.5-mL bed volume Ni-NTA column according to the manufacturer's instructions (Qiagen). Typically, 400 μg of purified protein was obtained.

AGG1 was purified from extracts using the following procedure. First, YFP-AGG1 was precipitated in the 20% to 40% NH_4SO_4 fraction. Samples were dialyzed against 50 mM NaH_2PO_4, pH 6.0, 2 mM β-mercaptoethanol, and 0.2% Tween 20. The dialyzed fractions were collected, and the YFP-AGG1 was purified over a 0.5-mL bed-volume DEAE-cellulose column, using a NaCl step gradient, according to the manufacturer's instructions (Qiagen). Typically, 500 μg of purified protein was eluted with the 200 mM NaCl fraction.

Membrane Flotation on Suc Step Gradients

For protein preparation, 100 mg of liquid N_2-frozen tissue was ground to powder with pestle and mortar. Total proteins (soluble and insoluble) were extracted by adding 1 mL of extraction buffer (50 mM HEPES-KOH, pH 7.5, 10 mM KCl, 5 mM EDTA, 5 mM EGTA, 10% Suc, 1 mg mL^{-1} phenylmethylsulfonyl fluoride, and protease inhibitor cocktail [Roche Diagnostics]) and incubated for 20 min on ice. Homogenates were precipitated at 3,000*g* for 10 min. The pellet was discarded, and the supernatant was collected for further analysis. To create a Suc step gradient, 250 μL of the supernatant was mixed with 1.25 mL of 85% Suc in TE buffer (10 mM Tris-HCl, pH 8.0, 1 mM EDTA, pH 8.0). This mixture was overlaid with 7 mL of 65% Suc and then 3 mL of 10% Suc in TE buffer. Centrifugal separation (4°C) was performed with an SW41 rotor (Beckman Coulter) at 100,000*g* for 18 h, followed by collecting 1.25-mL samples from the top of the gradient. Under these conditions, the membrane floated in fraction 3. To dilute the Suc, 3.75 mL of TE was added to each fraction and membranes were precipitated by centrifugation at 100,000*g* for 1 h. Membrane pellets were solubilized in 50 μL of 1% Triton X-100 in extraction buffer for 30 min on ice. To separate detergent-soluble and insoluble membranes, mixtures were centrifuged for 1 h at 100,000*g*. The pellet was solubilized by homogenization in 50 μL of 1% Triton X-100, 0.5% SDS in extraction buffer. Equal volumes of protein extracts in the detergent-soluble and insoluble membranes were resolved by SDS-PAGE (Laemmli, 1970), and proteins were identified by immunoblotting as described above.

Fractionation of AGG1

For protein fractionation, 100 mg of liquid N_2-frozen tissue was ground to powder with a pestle and mortar. Proteins were extracted by adding 300 μL of extraction buffer (50 mM NaH_2PO_4, pH 7.6, 300 mM NaCl, 10% glycerol, 2 mM β-mercaptoethanol, plant protease inhibitor mixture [Sigma], and 1 mg mL^{-1} phenylmethylsulfonyl fluoride) and incubated for 30 min on ice. To separate soluble and insoluble fractions, extracts were centrifuged at 100,000*g* for 60 min. The resulting supernatants representing the soluble fraction were collected for further analysis, and the insoluble pellet was incubated on ice for 30 min in the same volume (300 μL) of plant extraction buffer containing 1% Triton X-100 and 0.5% SDS. Extracts were centrifuged at 100,000*g* for 60 min. The resulting supernatant representing the membrane fraction was collected for further analysis.

Preparation of Samples for Analysis of Prenylation and *S*-Acylation by GC-MS

Analyses of prenylation and *S*-acylation were carried out essentially as described (Sorek et al., 2007; Sorek and Yalovsky, 2010). Briefly, 25 μg of purified His_6-GFP-rop6^{CA} or GFP-AGG1 protein was dried in a vacuum concentrator inside sealable glass vials (2-mL reactive vial; Whatman catalog no. 986276) and resuspended in formic acid:ethanol (1:4, v/v). Samples were washed three times with 0.5 mL of pentane:formic acid:ethanol (10:1:4, v/v) to remove noncovalently bound lipids. A total of 6.5 mg of platinum (IV) oxide was added per 400 μL of sample, and the proteins were hydrogenated for 90 min. Following hydrogenation, 70 mg of ethanol-washed Raney nickel (Fluka) was added (before use, 5 g of ready-to-use Raney nickel was washed 10 times with 50 mL of 100% ethanol), and cleavage was performed at 100°C for 16 h with continuous steering. Released lipids were extracted by adding 0.5 mL of pentane. This extraction was repeated three times, transferring the pentane into a new tube each time. The pentane washes were pulled and concentrated under N_2 to a final volume of 15 μL. Concentrated samples were analyzed by GC-MS.

Lipid Identification by GC-MS

GC-MS analysis was carried out as described previously (Sorek et al., 2007; Sorek and Yalovsky, 2010). Prenylation was detected by ion 71-monitored gel chromatograms, and acyl groups were detected by ion 101-monitored gel chromatograms. To monitor the prenyl lipids, the data were examined by GC-MS in single-ion mode. In the case of prenyl lipids, ion 71 represents the basic five-carbon isoprenoid unit.

Imaging

All images were produced with a Leica TCS-SL confocal laser scanning microscope (Leica Microsystems). GFP/YFP were excited with an argon laser at 488 nm, a 500-nm beam splitter, and the spectral detector set at 505 to 550 nm. FM4-64 was visualized by excitation with an argon laser at 514 nm and the spectral detector set between 530 and 560 nm. λ scans were carried out to verify the fluorescence emission spectra. All scans were carried out at 1,024- × 1,024-pixel resolution with repeated scanning of four lines. Scanning electron microscopy was carried out by direct analysis of sample, without fixation, and coating using a Hitachi TM 1000 (Hitachi High Technologies). Image analysis was carried out with Leica TCS, Zeiss LSM browser, Adobe Photoshop 7, and ImageJ.

Calculation of APS

Calculation of APS is based on measuring skeleton end points and circularity using ImageJ (Le et al., 2006). Cell structures were copied using ImageJ. The images were then filled and copied into a new blank image, which was then analyzed with the skeleton and circularity functions. APS was calculated with the following equation: APS = normalized skeleton + normalized circularity/2, where normalized skeleton = [(skeleton end points) – 2]/14 and normalized circularity = 1 – measured circularity.

FRAP Beam-Size Analysis

FRAP studies (Axelrod et al., 1976; Koppel et al., 1976) were carried out essentially as described previously (Illenberger et al., 2003; Henis et al., 2006; Eisenberg et al., 2008). FRAP measurements were carried out at 22°C on the abaxial side of cauline leaves taken from 2-week-old plants. The monitoring argon ion laser beam (488 nm, 1.2 μW) was focused through the microscope (AxioImager.D1; Carl Zeiss MicroImaging) to a spot with a Gaussian radius of 0.77 ± 0.03 μm (63×/1.4 numerical aperture oil-immersion objective) or 1.17 ± 0.05 μm (40×/1.2 numerical aperture water-immersion objective). FRAP experiments were conducted with each beam size as described (Illenberger et al., 2003; Henis et al., 2006), measuring 35 cells for each beam size. The ratio between the illuminated areas [$\omega^2(40\times)/\omega^2(63\times)$] was 2.28 ± 0.17 ($n$ = 59). After a brief measurement at the monitoring intensity, a 5-mW pulse (4–6 or 10–20 ms for the 63× and 40× objectives, respectively) bleached 50% to 70% of the fluorescence in the spot. Fluorescence recovery was followed by the monitoring beam. The apparent characteristic τ and the mobile fraction were derived from the FRAP curves by nonlinear regression analysis, fitting to a lateral diffusion process with a single τ value (Petersen et al., 1986). The significance of differences between τ values measured with the same laser beam size was evaluated by Student's t test. To compare ratio measurements [$\tau(40\times)/\tau(63\times)$ and $\omega^2(40\times)/\omega^2(63\times)$], we employed bootstrap analysis, which is preferable for comparison between ratio values (Efron and Tibshirani, 1993). The $\tau(40\times)$ and $\tau(63\times)$ values were resampled with replacement using Excel, and average values from each group of resampled data [$\tau(40\times)^{Boot}$ and $\tau(63\times)^{Boot}$] were derived. For each beam size, 1,000 averaged samples were generated, followed by calculation of the bootstrap ratio, dividing $\tau(40\times)^{Boot}$

by $\tau(63\times)^{Boot}$. To evaluate whether the τ ratios thus obtained differ significantly from the beam-size ratio calculated by the same method [$\omega^2(40\times)^{Boot}/\omega^2(63\times)^{Boot}$], the set of the τ bootstrap ratios was divided by the set of beam area bootstrap ratios, and the *P* value was derived from the spread of the resulting histogram around 1.

Mammalian Tissue Culture and Transfections

NIH3T3 cells were cultured in Dulbecco's modified Eagle's medium supplemented with 10% fetal calf serum in a 37°C/5% CO_2 incubator. Transfection into NIH3T3 cells was carried out with TransIT reagent (Mirus) using the manufacturer's instructions.

Immunostaining and Microscopy of Mammalian Cells

Cells were permeabilized with 3% paraformaldehyde and 0.5% Triton X-100 for 2 min and then mixed with 3% paraformaldehyde for an additional 30 min. Cells were washed with phosphate-buffered saline prior to immunostaining. Actin was stained with tetramethyl rhodamine isothiocyanate-phalloidin (Sigma P1951) and β-catenin with a polyclonal antibody (Sigma C2206) and a secondary antibody conjugated to Alexa 555 (Molecular Probes). Images were acquired with an IX81 Olympus microscope equipped with Hamamatsu's Orca C4742-80-12AG CCD camera.

Supplemental Data

The following materials are available in the online version of this article.

Supplemental Figure S1. GFP-ROP6 is localized to the plasma membrane.

Supplemental Figure S2. Quantification of the immunoblots from Figure 1B.

Supplemental Figure S3. MS spectra of prenyl and acyl lipids.

Supplemental Figure S4. Control GC chromatograms of AGG1 *S*-acylation.

Supplemental Figure S5. Quantification of pavement cell polarity.

Supplemental Figure S6. *ROP* gene expression microarray data.

Supplemental Movie S1. GFP-rop6^{CA}-induced membrane ruffles.

Supplemental Movie S2. His_6-GFP-rop6^{CA} in Col-0 cells.

Supplemental Movie S3. His_6-GFP-rop6^{CA} in *pggt-Ib* cells.

ACKNOWLEDGMENTS

We thank the Manna Center at the Department of Plant Sciences at Tel Aviv University for growth facilities support.

Received October 1, 2010; accepted November 30, 2010; published December 7, 2010.

LITERATURE CITED

Allen GJ, Murata Y, Chu SP, Nafisi M, Schroeder JI (2002) Hypersensitivity of abscisic acid-induced cytosolic calcium increases in the *Arabidopsis* farnesyltransferase mutant *era1-2*. Plant Cell **14:** 1649–1662

Armstrong SA, Hannah VC, Goldstein JL, Brown MS (1995) CAAX geranylgeranyl transferase transfers farnesyl as efficiently as geranylgeranyl to RhoB. J Biol Chem **270:** 7864–7868

Ausubel FM, Brent R, Kingston RE, Moore DD, Seidman JG, Smith JA, Struhl K (1995) Current Protocols in Molecular Biology. John Wiley & Sons, New York

Axelrod D, Koppel DE, Schlessinger J, Elson E, Webb WW (1976) Mobility measurement by analysis of fluorescence photobleaching recovery kinetics. Biophys J **16:** 1055–1069

Basu D, Le J, Zakharova T, Mallery EL, Szymanski DB (2008) A SPIKE1 signaling complex controls actin-dependent cell morphogenesis through the heteromeric WAVE and ARP2/3 complexes. Proc Natl Acad Sci USA **105:** 4044–4049

Belanis L, Plowman SJ, Rotblat B, Hancock JF, Kloog Y (2008) Galectin-1 is a novel structural component and a major regulator of h-ras nanoclusters. Mol Biol Cell **19:** 1404–1414

Berken A, Thomas C, Wittinghofer A (2005) A new family of RhoGEFs activates the Rop molecular switch in plants. Nature **436:** 1176–1180

Berken A, Wittinghofer A (2008) Structure and function of Rho-type molecular switches in plants. Plant Physiol Biochem **46:** 380–393

Bloch D, Lavy M, Efrat Y, Efroni I, Bracha-Drori K, Abu-Abied M, Sadot E, Yalovsky S (2005) Ectopic expression of an activated RAC in Arabidopsis disrupts membrane cycling. Mol Biol Cell **16:** 1913–1927

Bonetta D, Bayliss P, Sun S, Sage T, McCourt P (2000) Farnesylation is involved in meristem organization in Arabidopsis. Planta **211:** 182–190

Boulter E, Garcia-Mata R (2010) RhoGDI: a rheostat for the Rho switch. Small GTPases **1:** 65–68

Boulter E, Garcia-Mata R, Guilluy C, Dubash A, Rossi G, Brennwald PJ, Burridge K (2010) Regulation of Rho GTPase crosstalk, degradation and activity by RhoGDI1. Nat Cell Biol **12:** 477–483

Caldelari D, Sternberg H, Rodríguez-Concepción M, Gruissem W, Yalovsky S (2001) Efficient prenylation by a plant geranylgeranyltransferase-I requires a functional CaaL box motif and a proximal polybasic domain. Plant Physiol **126:** 1416–1429

Crowell DN, Huizinga DH (2009) Protein isoprenylation: the fat of the matter. Trends Plant Sci **14:** 163–170

Cutler S, Ghassemian M, Bonetta D, Cooney S, McCourt P (1996) A protein farnesyl transferase involved in abscisic acid signal transduction in Arabidopsis. Science **273:** 1239–1241

Díaz M, Sanchez Y, Bennett T, Sun CR, Godoy C, Tamanoi F, Duran A, Perez P (1993) The Schizosaccharomyces pombe cwg2+ gene codes for the β subunit of a geranylgeranyltransferase type I required for β-glucan synthesis. EMBO J **12:** 5245–5254

Efron B, Tibshirani R (1993) Estimates of bias. *In* DR Cox, DV Hinkley, N Reid, DB Rubin, BW Silverman, eds, An Introduction to Bootstrap. Chapman & Hall, London, pp 124–130

Efroni I, Eshed Y, Lifschitz E (2010) Morphogenesis of simple and compound leaves: a critical review. Plant Cell **22:** 1019–1032

Eisenberg S, Giehl K, Henis YI, Ehrlich M (2008) Differential interference of chlorpromazine with the membrane interactions of oncogenic K-Ras and its effects on cell growth. J Biol Chem **283:** 27279–27288

Farnsworth CC, Casey PJ, Howald WN, Glomset JA, Gelb MH (1990) Structural characterization of prenyl groups attached to proteins. Methods **1:** 231–240

Fowler JE (2010) Evolution of the ROP GTPase signaling module. *In* S Yalovsky, F Baluska, A Jones, eds, Integrated G Protein Signaling in Plants, Ed 1. Springer, Heidelberg, pp 305–327

Fu Y, Gu Y, Zheng Z, Wasteneys G, Yang Z (2005) Arabidopsis interdigitating cell growth requires two antagonistic pathways with opposing action on cell morphogenesis. Cell **120:** 687–700

Fu Y, Li H, Yang Z (2002) The ROP2 GTPase controls the formation of cortical fine F-actin and the early phase of directional cell expansion during *Arabidopsis* organogenesis. Plant Cell **14:** 777–794

Grizot S, Fauré J, Fieschi F, Vignais PV, Dagher MC, Pebay-Peyroula E (2001) Crystal structure of the Rac1-RhoGDI complex involved in NADPH oxidase activation. Biochemistry **40:** 10007–10013

Hazak O, Bloch D, Poraty L, Sternberg H, Zhang J, Friml J, Yalovsky S (2010) A rho scaffold integrates the secretory system with feedback mechanisms in regulation of auxin distribution. PLoS Biol **8:** e1000282

Henis YI, Rotblat B, Kloog Y (2006) FRAP beam-size analysis to measure palmitoylation-dependent membrane association dynamics and microdomain partitioning of Ras proteins. Methods **40:** 183–190

Hoffman GR, Nassar N, Cerione RA (2000) Structure of the Rho family GTP-binding protein Cdc42 in complex with the multifunctional regulator RhoGDI. Cell **100:** 345–356

Hordijk PL, ten Klooster JP, van der Kammen RA, Michiels F, Oomen LC, Collard JG (1997) Inhibition of invasion of epithelial cells by Tiam1-Rac signaling. Science **278:** 1464–1466

Hruz T, Laule O, Szabo G, Wessendrop F, Bleuler S, Oertle L, Widmayer P, Gruissem W, Zimmermann P (2008) Genevestigator V3: a reference expression database for the meta-analysis of transcriptomes. Adv Bioinformatics **2008:** 42074

Illenberger D, Walliser C, Strobel J, Gutman O, Niv H, Gaidzik V, Kloog Y, Gierschik P, Henis YI (2003) Rac2 regulation of phospholipase C-beta 2 activity and mode of membrane interactions in intact cells. J Biol Chem **278:** 8645–8652

Jaffe AB, Hall A (2005) Rho GTPases: biochemistry and biology. Annu Rev Cell Dev Biol **21:** 247–269

James GL, Goldstein JL, Brown MS (1995) Polylysine and CVIM sequences of K-RasB dictate specificity of prenylation and confer resistance to benzodiazepine peptidomimetic in vitro. J Biol Chem **270:** 6221–6226

Johnson CD, Chary SN, Chernoff EA, Zeng Q, Running MP, Crowell DN (2005) Protein geranylgeranyltransferase I is involved in specific aspects of abscisic acid and auxin signaling in Arabidopsis. Plant Physiol **139:** 722–733

Jones AM (2002) G-protein-coupled signaling in Arabidopsis. Curr Opin Plant Biol **5:** 402–407

Klahre U, Becker C, Schmitt AC, Kost B (2006) Nt-RhoGDI2 regulates Rac/Rop signaling and polar cell growth in tobacco pollen tubes. Plant J **46:** 1018–1031

Koppel DE, Axelrod D, Schlessinger J, Elson EL, Webb WW (1976) Dynamics of fluorescence marker concentration as a probe of mobility. Biophys J **16:** 1315–1329

Laemmli UK (1970) Cleavage of structural proteins during the assembly of the head of bacteriophage T4. Nature **227:** 680–685

Lavy M, Bloch D, Hazak O, Gutman I, Poraty L, Sorek N, Sternberg H, Yalovsky S (2007) A novel ROP/RAC effector links cell polarity, root-meristem maintenance, and vesicle trafficking. Curr Biol **17:** 947–952

Lavy M, Bracha-Drori K, Sternberg H, Yalovsky S (2002) A cell-specific, prenylation-independent mechanism regulates targeting of type II RACs. Plant Cell **14:** 2431–2450

Lavy M, Yalovsky S (2006) Association of Arabidopsis type-II ROPs with the plasma membrane requires a conserved C-terminal sequence motif and a proximal polybasic domain. Plant J **46:** 934–947

Le J, Mallery EL, Zhang C, Brankle S, Szymanski DB (2006) Arabidopsis BRICK1/HSPC300 is an essential WAVE-complex subunit that selectively stabilizes the Arp2/3 activator SCAR2. Curr Biol **16:** 895–901

Magee T, Seabra MC (2005) Fatty acylation and prenylation of proteins: what's hot in fat. Curr Opin Cell Biol **17:** 190–196

Maurer-Stroh S, Koranda M, Benetka W, Schneider G, Sirota FL, Eisenhaber F (2007) Towards complete sets of farnesylated and geranylgeranylated proteins. PLoS Comput Biol **3:** e66

Maurer-Stroh S, Washietl S, Eisenhaber F (2003) Protein prenyltransferases. Genome Biol **4:** 212

Michaelson D, Silletti J, Murphy G, D'Eustachio P, Rush M, Philips MR (2001) Differential localization of Rho GTPases in live cells: regulation by hypervariable regions and RhoGDI binding. J Cell Biol **152:** 111–126

Nagai T, Ibata K, Park ES, Kubota M, Mikoshiba K, Miyawaki A (2002) A variant of yellow fluorescent protein with fast and efficient maturation for cell-biological applications. Nat Biotechnol **20:** 87–90

Nibau C, Wu HM, Cheung AY (2006) RAC/ROP GTPases: 'hubs' for signal integration and diversification in plants. Trends Plant Sci **11:** 309–315

Niv H, Gutman O, Kloog Y, Henis YI (2002) Activated K-Ras and H-Ras display different interactions with saturable nonraft sites at the surface of live cells. J Cell Biol **157:** 865–872

Pei ZM, Ghassemian M, Kwak CM, McCourt P, Schroeder JI (1998) Role of farnesyltransferase in ABA regulation of guard cell anion channels and plant water loss. Science **282:** 287–290

Petersen NO, Felder S, Elson EL (1986) Measurement of lateral diffusion by fluorescence photobleaching recovery. *In* DM Weir, LA Herzenberg, CC Blackwell, LA Herzenberg, eds, Handbook of Experimental Immunology. Blackwell Scientific Publications, Edinburgh, pp 24.21–24.23

Prendergast GC (2001) Actin' up: RhoB in cancer and apoptosis. Nat Rev Cancer **1:** 162–168

Reid TS, Terry KL, Casey PJ, Beese LS (2004) Crystallographic analysis of CaaX prenyltransferases complexed with substrates defines rules of protein substrate selectivity. J Mol Biol **343:** 417–433

Reiss Y, Stradley SJ, Gierasch LM, Brown MS, Goldstein JL (1991) Sequence requirement for peptide recognition by rat brain $p21^{ras}$ protein farnesyltransferase. Proc Natl Acad Sci USA **88:** 732–736

Rotblat B, Prior IA, Muncke C, Parton RG, Kloog Y, Henis YI, Hancock JF (2004) Three separable domains regulate GTP-dependent association of H-ras with the plasma membrane. Mol Cell Biol **24:** 6799–6810

Running MP, Fletcher JC, Meyerowitz EM (1998) The *WIGGUM* gene is required for proper regulation of floral meristem size in *Arabidopsis*. Development **125:** 2545–2553

Running MP, Lavy M, Sternberg H, Galichet A, Gruissem W, Hake S, Ori N, Yalovsky S (2004) Enlarged meristems and delayed growth in *plp* mutants result from lack of CaaX prenyltransferases. Proc Natl Acad Sci USA **101:** 7815–7820

Sarojam R, Sappl PG, Goldshmidt A, Efroni I, Floyd SK, Eshed Y, Bowman JL (2010) Differentiating Arabidopsis shoots from leaves by combined YABBY activities. Plant Cell **22:** 2113–2130

Scheffzek K, Stephan I, Jensen ON, Illenberger D, Gierschik P (2000) The Rac-RhoGDI complex and the structural basis for the regulation of Rho proteins by RhoGDI. Nat Struct Biol **7:** 122–126

Seabra MC, Reiss Y, Casey PJ, Brown MS, Goldstein JL (1991) Protein farnesyltransferase and geranylgeranyltransferase share a common α subunit. Cell **65:** 429–434

Sjogren AK, Andersson KM, Liu M, Cutts BA, Karlsson C, Wahlstrom AM, Dalin M, Weinbaum C, Casey PJ, Tarkowski A, et al (2007) GGTase-I deficiency reduces tumor formation and improves survival in mice with K-RAS-induced lung cancer. J Clin Invest **117:** 1294–1304

Sorek N, Bloch D, Yalovsky S (2009) Protein lipid modifications in signaling and subcellular targeting. Curr Opin Plant Biol **12:** 714–720

Sorek N, Poraty L, Sternberg H, Bar E, Lewinsohn E, Yalovsky S (2007) Activation status-coupled transient S acylation determines membrane partitioning of a plant Rho-related GTPase. Mol Cell Biol **27:** 2144–2154

Sorek N, Segev O, Gutman O, Bar E, Richter S, Poraty L, Hirsch JA, Henis YI, Lewinsohn E, Jürgens G, et al (2010) An *S*-acylation switch of conserved G domain cysteines is required for polarity signaling by ROP GTPases. Curr Biol **20:** 914–920

Sorek N, Yalovsky S (2010) Analysis of protein *S*-acylation by gas chromatography-coupled mass spectrometry using purified proteins. Nat Protoc **5:** 834–840

Trueblood CE, Ohya Y, Rine J (1993) Genetic evidence for in vivo cross-specificity of the CaaX-box protein prenyltransferases farnesyltransferase and geranylgeranyltransferase-I in *Saccharomyces cerevisiae*. Mol Cell Biol **13:** 4260–4275

Uhlenbrock K, Eberth A, Herbrand U, Daryab N, Stege P, Meier F, Friedl P, Collard JG, Ahmadian MR (2004) The RacGEF Tiam1 inhibits migration and invasion of metastatic melanoma via a novel adhesive mechanism. J Cell Sci **117:** 4863–4871

Winge P, Brembu T, Bones AM (1997) Cloning and characterization of rac-like cDNAs from *Arabidopsis thaliana*. Plant Mol Biol **35:** 483–495

Wu G, Gu Y, Li S, Yang Z (2001) A genome-wide analysis of *Arabidopsis* Rop-interactive CRIB motif-containing proteins that act as Rop GTPase targets. Plant Cell **13:** 2841–2856

Yalovsky S, Bloch D, Sorek N, Kost B (2008) Regulation of membrane trafficking, cytoskeleton dynamics, and cell polarity by ROP/RAC GTPases. Plant Physiol **147:** 1527–1543

Yalovsky S, Kulukian A, Rodríguez-Concepción M, Young CA, Gruissem W (2000) Functional requirement of plant farnesyltransferase during development in *Arabidopsis*. Plant Cell **12:** 1267–1278

Yalovsky S, Trueblood CE, Callan KL, Narita JO, Jenkins SM, Rine J, Gruissem W (1997) Plant farnesyltransferase can restore yeast Ras signaling and mating. Mol Cell Biol **17:** 1986–1994

Yang Z (2008) Cell polarity signaling in Arabidopsis. Annu Rev Cell Dev Biol **24:** 551–575

Yang Z, Fu Y (2007) ROP/RAC GTPase signaling. Curr Opin Plant Biol **10:** 490–494

Zeng Q, Wang X, Running MP (2007) Dual lipid modification of Arabidopsis Gγ-subunits is required for efficient plasma membrane targeting. Plant Physiol **143:** 1119–1131

Ziegelhoffer EC, Medrano LJ, Meyerowitz EM (2000) Cloning of the Arabidopsis *WIGGUM* gene identifies a role for farnesylation in meristem development. Proc Natl Acad Sci USA **97:** 7633–7638